Volume 9 Issue 4 (2021) 301-305 ISSN 2347 - 3258
International Journal of Advance Research and Innovation

Measuring the Unsaturated Permeability Coefficient of Rock and Soil Masses with Self-developed Devices

Xin Liu[1,*], Teng Zhang[1], Hongyu Guo[2], Keyun Peng[2], Hongwei Zhang[2], Bo Tan[2], Runjie Lei[2]
[1]China Construction Fifth Engineering Division Corp, ltd, Hunan Changsha, 410031, China
[2]China Construction Infrastructure Co., ltd, Beijing, 100000, China

Article Info
Article history:
Received 25 October 2021
Received in revised form
20 November 2021
Accepted 28 November 2021
Available online 15 December 2021

Keywords
Rock and soil masses, On-site measurement, Testing device, Unsaturated permeability coefficient.

Abstract
To further study the unsaturated permeability coefficient of rock and soil masses, a model device for field testing the unsaturated permeability coefficient of rock and soil masses was developed, and a mathematical expression for field testing the unsaturated permeability coefficient was derived. By comparing and verifying with the test results, the results showed that the unsaturated permeability coefficient obtained from the field test of the device was very close to the existing test results and had a high accuracy. The device established in this paper can accurate determine the unsaturated permeability coefficient of rock and soil masses in the field, which has certain application value in engineering practice.

1. Introduction

Unsaturated rock and soil masses, that is, the pores between solid particles are partially filled with liquid, are a frequent presence in engineering practice. Rock and soil masses are a kind of natural geological material. The internal occurrences of defect structures, for instance, cracks, pores, joints and stratifications [1], not only change the mechanical properties of rock and soil masses, but also seriously affect their permeability characteristics [2]. In addition to be one of the most important hydraulic parameters of rock mass, permeability coefficient is a quantitative indicator of rock and soil permeability and a key index to characterize the permeability of rock and soil medium. Therefore, determining the unsaturated permeability coefficient of rock and soil masses is of great significance to engineering design, construction and safety.

However, accurately measuring the unsaturated permeability coefficient of rock and soil masses is by no means a simple matter for it is subject to many factors. Klute [3] first proposed the method of steady-state test to measure the unsaturated permeability coefficient of unsaturated soil. The permeability device for unsaturated soil developed by Chen et al. [4] provided good reference for the unsaturated permeability coefficient measurement. The joint tester for the unsaturated water-air motion invented by Liu et al. [5-8] afforded us insightful data for the study of unsaturated permeability coefficient. Based on unsaturated soil theory, Shao et al. [9-11] developed a joint measuring instrument for soil-water characteristic curve and permeability coefficient, which can effectively shorten test time and improve the measurement accuracy of permeability coefficient. Some researchers, such as Huang et al. [12], Samingan et al. [13] and Xu et al. [14], further developed the triaxle permeability apparatus, which contributed a lot to the research of unsaturated permeability coefficient. Currently, there are two approaches to determine the permeability coefficient of rock mass, namely, on-site hydraulic testing [15] and empirical estimation [16]. Widely applied in rock mass engineering, in particular in hydrogeological survey of large-scale construction sites, on-site hydraulic testing method can be classified into pumping test and packer permeability test [17]. Without taking the disturbance to rock and soil masses into consideration in their unsaturated permeability coefficient measurement, most of the above-mentioned studies are highly like to yield errors.

***Corresponding Author,**
E-mail address: wrc05092021@163.com

Targeted at these problems, we developed a set of devices for the on-site measurement of the unsaturated permeability coefficient of rock and soil masses. The mathematical expression of unsaturated permeability coefficient measurement was derived on the basis of the GA model. The obtained value of unsaturated permeability coefficient was then compared with the existing experimental data. The results show that the two figures were very close. Therefore, the unsaturated permeability coefficient measured by the devices is reliable and accurate.

2. Test device and experimental process

2.1. Test device

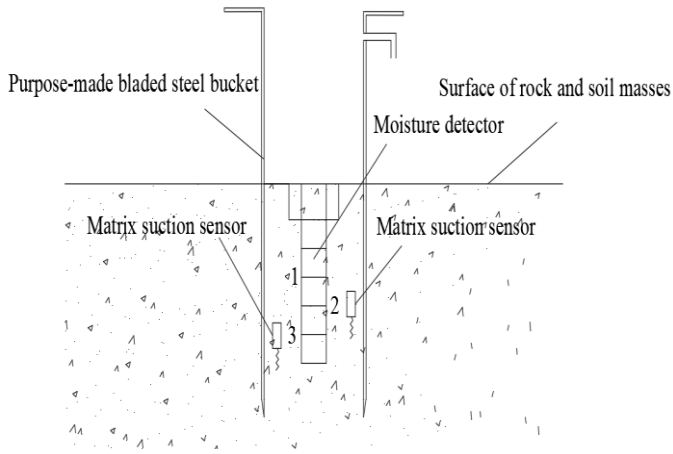

Fig. 1: Schematic diagram of test device

Figure 1 shows the device for the on-site unsaturated permeability coefficient measurement of rock and soil masses. The gadget is composed of moisture detector, matrix suction sensor, data collector, drilling tools and bladed steel bucket. The following are the detailed description of the major components:

2.1.1 Moisture detector

With a total height of 35cm, moisture detector has 6 sections. The height of the first section is 10cm, and each of the remaining five sections is of the same height (5 cm). Figure 2 shows the structural diagram of moisture detector. On the helix part is a threaded wave conductor. It has two functions: one is to improve the contact between sensor and soil; the other is to prevent the error caused by the dominant flow around sensor and air gap around the waveguide rod. The moisture detector can be applied to measure volume water content (VWC), conductivity (EC) and temperature within the rock and soil masses at different depths.

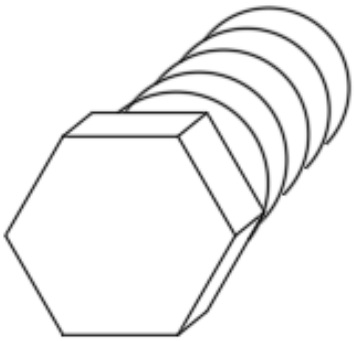

Fig. 2: Structural diagram of moisture detector

2.1.2 Matric suction sensor

Figure 3 shows the structural diagram of matric suction sensor. The top of the sensor is cylindrical. The helix structure equipped at the bottom is used to screw the matrix suction sensor into the rock and soil masses. The sensor is capable of monitoring the matric suction values near the rock and soil masses at different depths.

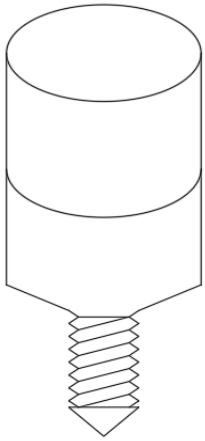

Fig. 3: Structural diagram of matric suction sensor

2.1.3 Purpose-made bladed steel bucket

With a height of 85cm, the bucket has an inner diameter of 120mm and an outer diameter of 140mm. Figure 4 shows its structure diagram. The top and bottom of the bucket are open. There is an extension of 15cm on both sides of the top. Helping to press the bucket into the rock and soil masses, both sides of the blade-shaped bottom is applied to fix a certain area. A notch 5cm away from the top is connected with the outside environment. Thus, the water surface can be maintained at a certain height, and the surface of rock and soil masses is always in a ponding state.

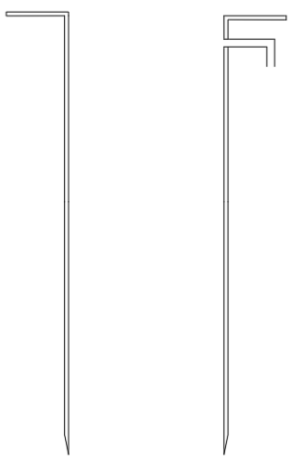

Fig. 4: Structure diagram for the purpose-made bladed bucket

3. Experimental process

(1) Enclose part of the rock and soil masses with the bladed steel bucket, then a water reservoir is formed above the rock and soil masses. Install the moisture detector, which is linked to data collectors, in the rock and soil masses. The top end of the moisture detector is parallel to the surface of rock and soil masses.
(2) Install multiple matrix suction sensors, which are connected to the data collectors, in the rock and soil masses. Make sure these sensors are located at different depths around the moisture detector, so that the detection range of the sensors can cover the area around the moisture detector.
(3) Continuously inject water into the water reservoir until the water level reaches the set height. Discharge water at the same time, so that the water level in the reservoir is maintained at the set level.
(4) Select a monitoring section and a time period from t_1 to t_2 after water seeps below the monitoring section. Through the data collectors, gather the data of the moisture detector and matrix suction sensors. Analyze and process the test data, then we got the unsaturated permeability coefficient of rock and soil masses from T_1 to T_2 .

4. Calculation of permeability coefficient

Figure 5 is the schematic diagram for the immersion peak motion when water infiltrates from the upper-end to the lower-end of the vertical soil column under the ponding condition. Let us suppose that point A is the bottom section of rock and soil masses, and point B (No. 1 sensing position) is the monitoring section of rock and soil masses, then the infiltration peak develops to cross-sections N_1 (No. 2 sensing position) and N_2 (No. 3 sensing position) when the ponding durations are T_1 and T_2 respectively.

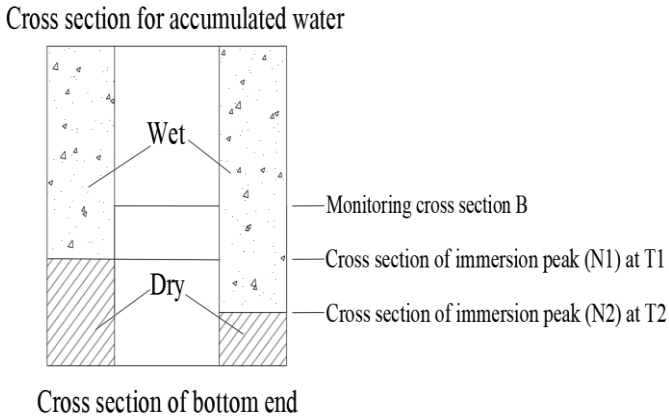

Fig. 5: Schematic diagram for the motion of immersion peak

On the basis of the permeability coefficient of unsaturated soil derived by Qin et al. [18], we know that:

$$k = \frac{\left\{0.5\left[\Phi\left(h_B, t_2\right) + \Phi\left(h_B, t_1\right)\right] - \Phi_0\right\}\gamma_w v^2}{\left[\psi\left(h, t_1\right) - \psi\left(h, t_2\right) - \gamma_w v\left(t_2 - t_1\right)\right]} \quad (1)$$

According to the infiltration equation of GA model [19]:

$$q = k_s \frac{h_f + H + \psi_f}{h_f} \quad (2)$$

In the equation: q represents infiltration rate; k_s is the saturated permeability coefficient of rock and soil masses; h_f stands for the infiltration depth (immersion peak), or, the thickness of saturation zone; H is the water-collection layer thickness on the surface of the rock and soil masses; ψ_f represents the matrix suction water head size of the rock and soil masses on the boundary line.

The above GA model presupposes that the water content of rock and soil masses in the saturated zone above the immersion peak is completely saturated, which is, in fact, not the case. In accordance with the actual size of water contents, researchers conducted a

large number of experiments and divided the saturated zone into two parts: fully saturated section and transition section (Figure 6 and Figure 7). The thickness of both accounts for half of that of the saturation zone [20]. The water content distribution curve of the transition layer can be expressed with the elliptic curve. On the basis of the above hypothesis, the expression of water content distribution in the slope after rainwater infiltration is as follows:

$$\Phi=\begin{cases}\Phi_s & 0\le h\le h_s\\ \Phi_i+(\Phi_s-\Phi_i)\sqrt{1-\left(\dfrac{h-h_s}{h_s}\right)} & h_s<h<h_f\\ \Phi_i & h\ge h_f\end{cases} \quad (3)$$

In the equation: the dependent variable Φ represents water contents; the independent variable h stands for depth. Φ_i is the initial water content; Φ_s is the saturated water content; h_s symbolizes the thicknesses of fully saturated layer and transition layer, $h_s=h_f/2$

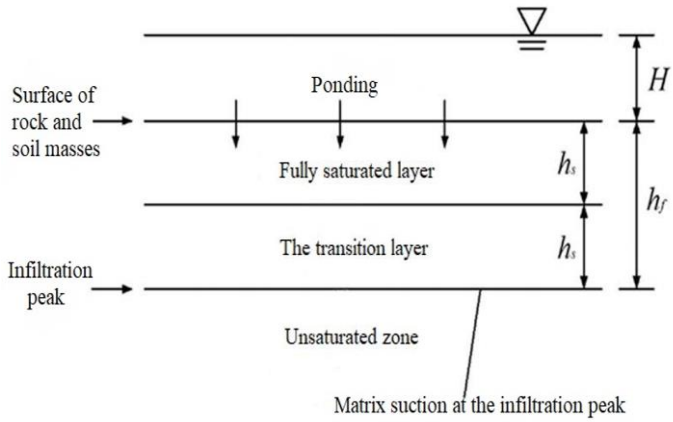

Fig. 6: Green-Ampt layer infiltration model

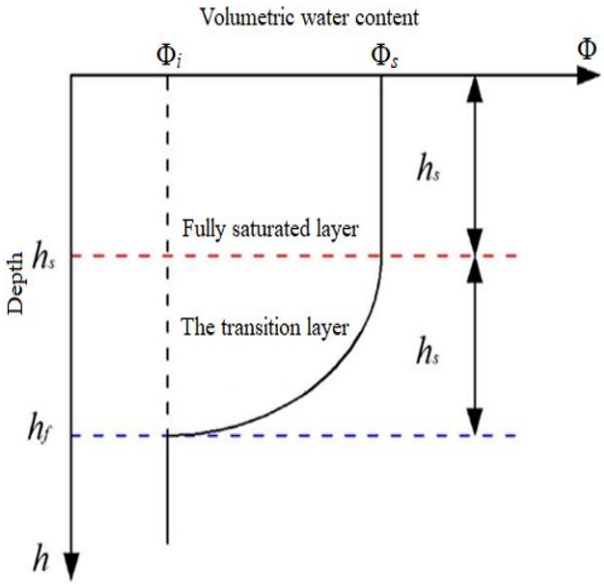

Fig. 7: Cross-sectional diagram for water content distribution at the saturated zone

In accordance with Eq(3), we derived the total infiltration amount of ponding water corresponding to any water accumulation time t.

(4)

$$I=(\Phi_s-\Phi_i)h_s+\int_{h_s}^{h_f}(\Phi-\Phi_i)dh$$
$$=(\Phi_s-\Phi_i)\frac{h_f}{2}+\int_{\frac{h_f}{2}}^{h_f}(\Phi_s-\Phi_i)\sqrt{1-\left(\frac{h-h_s}{h_s}\right)^2}dh$$
$$=\frac{(4+\pi)(\Phi_s-\Phi_i)h_f}{8}$$

In the equation, I is the total infiltration quantity at the time of water accumulation, Φ_i is the initial water content; Φ_s is the saturated water content.

Supposing the infiltration depth is h_f' at a certain time t_1, then the infiltration amount of ponding is equal to the total infiltration amount.

$$(\Phi_s-\Phi_i)h_f'=I=\frac{(4+\pi)(\Phi_s-\Phi_i)h_f}{8} \quad (5)$$

From Eq(2), we know that the infiltration rate at the time of t_1 is $q'=k_s\dfrac{h_f'+H+\psi_f}{h_f'}$, and $q'=\dfrac{dI'}{dt}$

$$dI'=q'dt=k_s\frac{h_f'+H+\psi_f}{h_f'}dt \quad (6)$$

Substitute Eq(5) into Eq(7), then:

$$d\frac{(4+\pi)(\Phi_s-\Phi_i)h_f'}{8}=k_s\frac{h_f'+H+\psi_f}{h_f'}dt \quad (7)$$

Eq(7) is reduced as:

$$\frac{(4+\pi)(\Phi_s-\Phi_i)h_f'}{8k_s(h_f'+H+\psi_f)}dh_f'=dt \quad (8)$$

Integrate both sides of Eq(9) over t, then

$$\int\frac{(4+\pi)(\Phi_s-\Phi_i)h_f'}{8k_s(h_f'+H+\psi_f)}dh_f'=\int dt \quad (9)$$

$$\frac{(4+\pi)(\Phi_s-\Phi_i)}{8k_s}\left[h_f'-(H+\psi_f)l_n(h_f'+H+\psi_f)\right]=t+C$$

(10)

In the equation, C is an arbitrary constant. The height of the infiltration h_f' equals to 0 when time t is 0. Thus,

$$C=-\frac{(4+\pi)(\Phi_s-\Phi_i)(H+\psi_f)l_n(H+\psi_f)}{8k_s} \quad (11)$$

Substitute Eq(12) into Eq(11), then we obtain the expression of infiltration height h_f' and time t:

$$t=\frac{(4+\pi)(\Phi_s-\Phi_i)\left\{h_f'+(H+\psi_f)\left[l_n(H+\psi_f)-l_n(h_f'+H+\psi_f)\right]\right\}}{8k_s}$$

(12)

Therefore, the motion rate of infiltration peak (v) is:

$$v=\frac{\Delta h}{\Delta t}=\frac{h_f'}{t}=\frac{8k_sh_f'}{(4+\pi)(\Phi_s-\Phi_i)\left\{h_f'+(H+\psi_f)\left[l_n(H+\psi_f)-l_n(h_f'+H+\psi_f)\right]\right\}}$$

(13)

Substitute Eq(14) into Eq(1), then we work out the unsaturated permeability coefficient k:

$$k=\frac{\left\{0.5\left[\Phi\left(h_B,\ t_2\right)+\Phi\left(h_B,\ t_1\right)\right]-\Phi_0\right\}\gamma_w\dfrac{8k_sh_f^{'}}{(4+\pi)(\Phi_s-\Phi_i)\left\{h_f^{'}+\left(H+\psi_f\right)\left[l_n\left(H+\psi_f\right)-l_n\left(h_f^{'}+H+\psi_f\right)\right]\right\}}}{\left[\psi\left(h,\ t_1\right)-\psi\left(h,\ t_2\right)-\gamma_w\left(t_2-t_1\right)\dfrac{8k_sh_f^{'}}{(4+\pi)(\Phi_s-\Phi_i)\left\{h_f^{'}+\left(H+\psi_f\right)\left[l_n\left(H+\psi_f\right)-l_n\left(h_f^{'}+H+\psi_f\right)\right]\right\}}\right]}^2 \quad (14)$$

Wherein k_s is the saturated permeability coefficient of the rock and soil masses, $h_f^{'}$ is the depth of infiltration peak at any time, $\Phi\left(h_B,t_2\right)$ is the volumetric moisture content for point B at the moment of t_2, $\Phi\left(h_B,t_1\right)$ is the volumetric moisture content for point B at the moment of t_1, Φ_0 is the initial volume moisture content of the rock and soil masses, γ_w is density of water, $\psi\left(h,\ t_1\right)$ is the size of matric suction at the moment of t_1, $\psi\left(h,\ t_2\right)$ is the size of matric suction at the moment of t_2.

5. Verification of testing results

To verify our testing results, we compared the unsaturated permeability coefficient derived from the on-site tests with the parallel experimental results (see No. 21 of the References). The purpose is to compare with the existed experimental results to prove the reasonableness of the equation in the derivation process of this paper. The 240-min parallel experiment was conducted by Lin et al. on a loess layer of Nanyuan irrigation area, Jingyang, Shaanxi Province. The relevant physical parameters are shown in Table 1.

Table 1: Relevant physical parameters for unsaturated loess

q	ψ_f	H	$h_f^{'}$	Φ_0
8.9×10^{-3}cm/s	5714cm	10.5cm	57cm	10.4%
$\Phi\left(h_B,t_1\right)$	$\Phi\left(h_B,t_2\right)$	$\psi\left(h,\ t_1\right)$	$\psi\left(h,\ t_2\right)$	γ_w
10.4%	27.34%	652KPa	0	10KN /m^3

On the basis of the above data and Eq(2), the saturated permeability coefficient of the loess was calculated to be 1.95×10^{-3} cm/s. According to Lin et al. [21], the saturation permeability coefficient is within the reasonable range of 1.8×10^{-3}cm/s ~ 2.0×10^{-3}cm/s, thus indicating that the equations in the derivation process of this paper are reasonable and correct. It shows that our calculation results are reasonable and correct. However, Lin et al. is based on the regularity and results of the loess infiltration test, proposing the method of determining the saturation permeability coefficient of the soil in the field, the determination process produces certain disturbance to the soil and the method has limitations in the determination of other soils. In contrast, the device for field testing of permeability coefficient in the paper has less disturbance to the soil during the determination process, and the determination range is more comprehensive, which can determine not only the permeability coefficient of soil but also the permeability coefficient of rock masses.

On the basis of Eq(15), the unsaturated permeability coefficient of the loess was calculated to be 3.35×10^{-5}cm/s, it is very close to the unsaturated permeability coefficient of 3.5×10^{-5}cm/s in Lin et al. [21]. It once again proves that the unsaturated permeability coefficient measured by this test device is reliable and has a high accuracy.

6. Conclusions

This study developed a set of model devices for the on-site unsaturated permeability coefficient measurement of rock and soil masses. In addition to the advantages of simple supporting components, low cost, easy operation, the device is capable of measuring a great diversity of parameters. With slight disturbance to the rock and soil masses during its working process, it objectively reflect the real permeability coefficient of the rock and soil masses.

By comparing the unsaturated permeability coefficient value obtained by the device with the experimental results, we proved that the measurement figure is very close to the experimental results. Achieving the actual measurement accuracy, the self-developed device is of great significance to the calculation of unsaturated permeability coefficient of rock and soil masses in engineering practice.

References

[1]. ZL Li, QW Ren. Analysis and discussion of hydraulic fracturing of rock mass concrete under the action of natural construction force. Rock and Soil Mechanics, 29(8), 2018, 2121-2125. DOI: 10.3969/j.issn.1000-7598.2008.08.020

[2]. ZP Sun, ZN Gao, XR Meng. On the permeability coefficient of surrounding rock damage zone based on Drucker Prager criterion. Journal of Yangtze River Scientific Research Institute, 30(3), 2013, 26-29+39. DOI: 10.3969/j.issn.1001-5485.2013.03.006

[3]. A Klute. Laboratory Measurement of Hydraulic Conductivity of Saturated Soil, Methods, 1965. DOI: 10.2134/agronmonogr9.1.c16

[4]. ZH Chen, D Xie, YS Wang. On the Law of Water and Air Movement in Unsaturated Soil and Its Engineering Properties. Chinese Journal of Geotechnical Engineering, (3), 1993, 9-20. DOI: 10.1007/bf02656947

[5]. Z Zhang, FY Liu, JL Qi, et al. Characterization of unsaturated seepage anisotropy of soil based on pore connectivity and tortuosity parameters, Chinese Journal of Geotechnical Engineering, 40(S1), 2018, 147-152. DOI: 10.11779/cjge2018s1024

[6]. FY Liu, Z Zhang, D Zhou, et al. The influence of density and dry-wet cycle on the soil-water characteristic curve of loess. Rock and Soil Mechanics, 32(S2), 2011, 132-136. DOI: cnki:sun:ytlx.0.2011-S2-021

[7]. FY Liu, Z Zhang, D Zhou, et al. Permeability Function of Unsaturated Loess under the Conditions of Changing Humidity and Density, Journal of Hydraulic Engineering, 41(9), 2010, 1054-1060. DOI: cnki:sun:slxb.0.2010-09-008

[8]. FY Liu, Z Zhang, D Zhou, et al. Permeability Function of Unsaturated Loess under the Conditions of Changing Humidity and Density. Chinese Journal of Rock Mechanics and Engineering, 29(9), 2010, 1907-1914. DOI: cnki:sun:yslx.0.2010-09-022

[9]. AM Liang. An Experimental Study on the Infiltration Characteristics and Saturated Infiltration Mechanism of Unsaturated Soil, Dalian. Dalian University of Technology, 2008.

[10]. LT Shao, AM Liang, ZP Wang, et al. Manufacture and application of steady seepage equipment for unsaturated soil. Chinese Journal of Geotechnical Engineering, (11), 2005, 103-105. DOI: 10.3321/j.issn:1000-4548.2005.11.021

[11]. J Sun. On the Soil-Water Characteristic Curve and Water Conductivity Measurement Method of Unsaturated Soil, Dalian. Dalian University of Technology, 2001.

[12]. S Huang, DG Fredlund, SL Barbour. Measuring the permeability coefficient for a deformable unsaturated soil. Canadian Geotechnical Journal, 35(3), 1998, 426-432. DOI: 10.1139/cgj-35-3-426

[13]. AS Samingan, EC Leong, H Rahardjo. A flexible wall permeameter for the measurement of water and air permeability

coefficients of residual soils. Canadian Geotechnical Journal, 40(3), 2003, 559-574. DOI: 10.1139/t03-015
[14]. YF Xu, SQ Lan, DA Sun, et al. Measuring the influence of stress state on the permeability coefficient of unsaturated soil with a new device. Chinese Journal of Rock Mechanics and Engineering, 24(2), 2005, 160-164. DOI: 10.3321/j.issn:1000-6915.2005.01.027
[15]. X Tu, YW Zeng, DY Tang. The permeability coefficient of rock mass based on underwater pumping test and its application. Chinese Journal of Rock Mechanics and Engineering, 29(S2), 2010, 3542-3548.
[16]. CY Ku, SM Hsu, LB Chiou, et al. An empirical model for estimating hydraulic conductivity of highly disturbed clastic sedimentary rocks in Taiwan. Engineering Geology-Amsterdam, 109(3), 2009, 213-223. DOI: 10.1016/j.enggeo.2009.08.008
[17]. JQ Guo, Y Li, HS Wang, et al. Linear regression method for identifying aquifer parameters and position of straight line recharge boundary., Journal of Hydraulic Engineering, 37(6), 2006, 807-812. DOI: 10.3321/j.issn:0559-9350.2006.07.007
[18]. XH Qin, DS Liu, QH Song, et al. On the vertical infiltration test of One-dimensional soil column and solution of its permeability coefficient under rainfall conditions. Chinese Journal of Rock Mechanics and Engineering, 36(2), 2017, 475-484. DOI: 10.13722/j.cnki.jrme.2016.0068
[19]. WH Green, GA Ampt. Studies on Soil Physics. The Journal of Agricultural Science, 4(1), 1911, 1-24.
[20]. WY Wang, ZR Wang, J Quan, et al. Improvement and evaluation of the Green-Ampt model in loess. Journal of Hydraulic Engineering, (5), 2003, 30-34. DOI: 10.3321/j.issn:0559-9350.2003.05.005
[21]. HZ Lin, JB Peng, H Yang, et al. A simple estimation approach for the saturated permeability of loess in field by a double-ring infiltrometer. Advances in Water Science, 28(4), 2017, 523-533. DOI: 10.14042/j.cnki.32.1309.2017.04.006